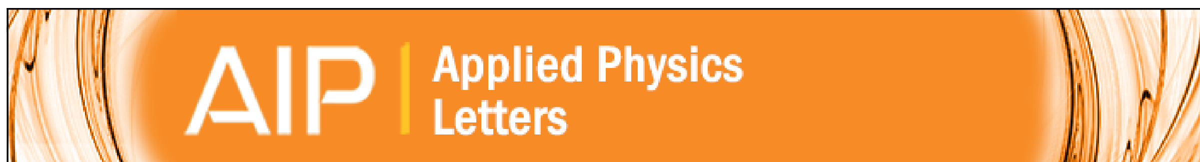

Direct growth of hexagonal boron nitride/graphene heterostructures on cobalt foil substrates by plasma-assisted molecular beam epitaxy

Zhongguang Xu, Alireza Khanaki, Hao Tian, Renjing Zheng, Mohammad Suja, Jian-Guo Zheng, and Jianlin Liu

Citation: Applied Physics Letters **109**, 043110 (2016); doi: 10.1063/1.4960165
View online: http://dx.doi.org/10.1063/1.4960165
View Table of Contents: http://scitation.aip.org/content/aip/journal/apl/109/4?ver=pdfcov
Published by the AIP Publishing

Articles you may be interested in

Direct growth of graphene on in situ epitaxial hexagonal boron nitride flakes by plasma-assisted molecular beam epitaxy
Appl. Phys. Lett. **107**, 213103 (2015); 10.1063/1.4936378

Synthesis of atomically thin hexagonal boron nitride films on nickel foils by molecular beam epitaxy
Appl. Phys. Lett. **106**, 213108 (2015); 10.1063/1.4921921

Direct growth of nanocrystalline hexagonal boron nitride films on dielectric substrates
Appl. Phys. Lett. **106**, 101901 (2015); 10.1063/1.4914474

A cohesive law for interfaces in graphene/hexagonal boron nitride heterostructure
J. Appl. Phys. **115**, 144308 (2014); 10.1063/1.4870825

Interlayer coupling enhancement in graphene/hexagonal boron nitride heterostructures by intercalated defects or vacancies
J. Chem. Phys. **140**, 134706 (2014); 10.1063/1.4870097

NEW Special Topic Sections
NOW ONLINE
Lithium Niobate Properties and Applications: Reviews of Emerging Trends
AIP Applied Physics Reviews

Reuse of AIP Publishing content is subject to the terms at: https://publishing.aip.org/authors/rights-and-permissions. Download to IP: 169.235.13.190 On: Fri, 29 Jul 2016 21:22:09

Direct growth of hexagonal boron nitride/graphene heterostructures on cobalt foil substrates by plasma-assisted molecular beam epitaxy

Zhongguang Xu,[1] Alireza Khanaki,[1] Hao Tian,[1] Renjing Zheng,[1] Mohammad Suja,[1] Jian-Guo Zheng,[2] and Jianlin Liu[1,a)]
[1]*Quantum Structures Laboratory, Department of Electrical and Computer Engineering, University of California, Riverside, California 92521, USA*
[2]*Irvine Materials Research Institute, University of California, Irvine, California 92697-2800, USA*

(Received 11 May 2016; accepted 20 July 2016; published online 29 July 2016)

Graphene/hexagonal boron nitride (G/h-BN) heterostructures have attracted a great deal of attention because of their exceptional properties and wide variety of potential applications in nanoelectronics. However, direct growth of large-area, high-quality, and stacked structures in a controllable and scalable way remains challenging. In this work, we demonstrate the synthesis of h-BN/graphene (h-BN/G) heterostructures on cobalt (Co) foil by sequential deposition of graphene and h-BN layers using plasma-assisted molecular beam epitaxy. It is found that the coverage of h-BN layers can be readily controlled on the epitaxial graphene by growth time. Large-area, uniform-quality, and multi-layer h-BN films on thin graphite layers were achieved. Based on an h-BN (5–6 nm)/G (26–27 nm) heterostructure, capacitor devices with Co(foil)/G/h-BN/Co(contact) configuration were fabricated to evaluate the dielectric properties of h-BN. The measured breakdown electric field showed a high value of ~2.5–3.2 MV/cm. Both I-V and C-V characteristics indicate that the epitaxial h-BN film has good insulating characteristics. *Published by AIP Publishing.*
[http://dx.doi.org/10.1063/1.4960165]

Hexagonal boron nitride (h-BN) is an excellent two-dimensional (2D) dielectric layer and has been studied intensively not only for its exceptional properties but also for its compatibility with graphene (G) and other 2D material systems.[1–10] Recently, much work has been done on the assembly of both lateral and vertical G/h-BN heterostructures.[11–21] Such heterostructures have provided a platform to investigate novel phenomena in fundamental physics such as Hofstadter butterfly effect and quantum Hall effect[22,23] and to develop a variety of nanodevices with superior performance.[3,10,24] For example, graphene-based transistors using h-BN as a gate insulator and supporting substrate have shown significantly enhanced field-effect carrier mobility in part due to its atomically flat and dangling-bond-free h-BN surfaces, which greatly reduce charge scattering centers at the G/h-BN interfaces.[9,11]

Traditionally, both graphene and h-BN films can be obtained by the mechanical exfoliation method and assembled into heterostructures.[25] Although this method can result in crystalline flakes and layered samples, the thickness and size of such samples are difficult to control. On the other hand, chemical vapor deposition (CVD) has been used to provide an alternative approach for the preparation of h-BN/G heterostructures. For example, CVD growth of h-BN (or G) on mechanically exfoliated G (or h-BN) as well as two-step CVD growth for both G and h-BN have been reported to obtain h-BN and graphene-based heterostructures.[11–14,22] Although significant progress has been made for these heterostructures, it is still challenging to controllably and scalably synthesize large-area, high-quality layers. MBE is an alternative tool and has natural advantages in high-quality layer-by-layer film deposition thanks to its ultra-high vacuum (UHV) environment, atomic layer epitaxy accuracy and controllability, instant introduction and control of multiple sources, ease of doping of materials and *in-situ* layer-by-layer characterization. In particular, MBE is promising for the *in-situ* growth of vertically stacked heterostructures with defect-free interfaces due to the catalytic-free processes since the existing as-grown layers will serve as a template for sequential growth.[26] As a matter of fact, the 2D material field is experiencing a surge in using MBE for graphene and BN research; for example, MBE has been used to successfully synthesize graphene and h-BN films on cobalt and nickel thin film substrates.[27–31] More recently, nickel foil has been used to synthesize atomically thin h-BN films by MBE.[26] In this paper, we report MBE growth of large-area, uniform-quality, and vertically stacked h-BN/G heterostructures on cobalt foil. In addition, capacitor devices with Co(foil)/G/h-BN/Co(contact) structure were fabricated to evaluate dielectric properties of the h-BN films.

First, cobalt foils (Alfa Aesar, 0.1 mm thick, 99.995%) were cut into 1 cm × 1 cm pieces as substrates. A re-designed Perkin-Elmer MBE system was used for sample growth. A Knudsen effusion cell filled with B_2O_3 powder (Alfa Aesar, 99.999%) was used as a boron (B) source. Nitrogen plasma (Airgas, 99.9999%) was generated by an electron cyclotron resonance (ECR) system as a nitrogen (N) source. Acetylene gas (Airgas, 99.999%) was used as a carbon (C) source.

A Co foil substrate was cleaned with diluted hydrochloric acid (10%) in order to remove the native oxide layer, rinsed with deionized (DI) water, blown dry, and then immediately loaded into the MBE chamber. First, the substrate was heated to 850 °C and annealed at this temperature under 10-standard cubic centimeters per minute (sccm) flow of

[a)]Author to whom correspondence should be addressed. Electronic mail: jianlin@ece.ucr.edu. Tel.: 1-9518277131. Fax: 1-9518272425.

Reuse of AIP Publishing content is subject to the terms at: https://publishing.aip.org/authors/rights-and-permissions. Download to IP: 169.235.13.190 On: Fri, 29 Jul 2016 21:22:09

hydrogen (H_2) gas for a duration of 20 min. Then, the graphene growth started by introducing 3-sccm acetylene (C_2H_2) gas and 6-sccm H_2 gas, and lasted for 60 s. Immediately after the graphene growth, h-BN growth started at the same substrate temperature. During the growth, the B cell temperature was kept at 1150 °C, and 10-sccm N_2 through an ECR source along with 6-sccm H_2 was introduced into the chamber. The ECR current was set at 60 mA with a power of 228 W, and the growth took 5, 20, and 30 min for three samples, respectively. Finally, the substrate was cooled to room temperature at a rate of 10 °C/min. A reference sample, i.e., multilayer graphene without h-BN on top was also grown on a Co foil with the same growth condition. Supplementary material Figure S1 shows schematic of the growth process of an h-BN/G heterostructure.

Co(foil)/G/h-BN/Co(contact) capacitor devices were fabricated by standard photolithography and lift-off processes. A Co layer of 100 nm was patterned to form top contacts with a size of 250 μm × 250 μm on the surface of the as-grown h-BN/G film. Reactive ion etching (RIE) with 50-sccm SF_6 plasma under a power of 50 W was carried out for 15 s to etch the h-BN/G film between devices, which ensures isolation of different devices on the same substrate.

Raman characterizations were performed using a HORIBA LabRam system equipped with a 50-mW 514-nm green laser. Scanning electron microscopy (SEM) images were acquired using an XL30-FEG SEM system. X-ray photoelectron spectroscopy (XPS) characterization was carried out using a Kratos AXIS ULTRA XPS system equipped with an Al Kα monochromatic X-ray source and a 165-mm mean radius electron energy hemispherical analyzer. Absorption spectra were measured by a Varian Cary 500 double-beam scanning ultraviolet/visible/near-infrared spectrophotometer. Atomic force microscopy (AFM) images were obtained using a Veeco D3100 AFM system. Transmission electron microscopy (TEM) images were acquired using an FEI/Philips CM-20 TEM. Cross-sectional TEM samples were prepared using the focused ion beam technique. The h-BN/G thin film was covered first by an amorphous carbon protection layer and further by electron-beam and ion-beam deposited Pt protection layers. Transferred samples on either SiO_2-coated Si or sapphire substrates were obtained by a PMMA-assisted method.[28,29] Current-voltage (I-V) characteristics were obtained by an Agilent 4155C semiconductor parameter analyzer. Capacitance-voltage (C-V) characteristics were obtained by an Agilent 4284A LCR meter.

Figure 1(a) shows an SEM image of the as-grown graphene on cobalt foil, i.e., the reference sample (Sample A), presenting a large-scale continuous film. Figs. 1(b)–1(d) show SEM images of the as-grown h-BN/G heterostructure

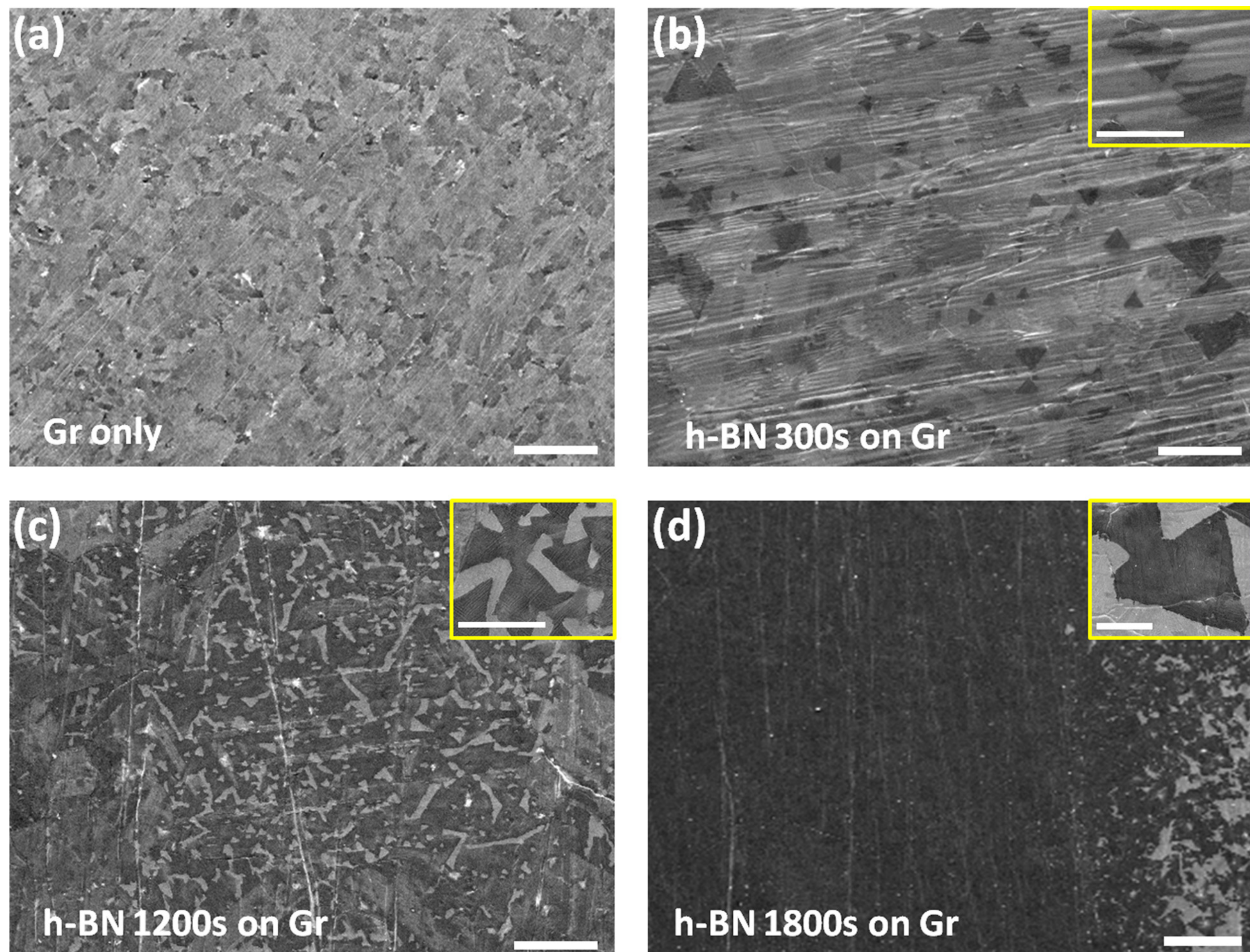

FIG. 1. SEM image of (a) the graphene (G) on Co foil (Sample A); and h-BN on G film at different h-BN layer growth times: (b) 300 s (Sample B), (c) 1200 s (Sample C), and (d) 1800 s (Sample D). Insets in (b), (c), and (d) are magnified SEM images of local surface areas of these samples. Scale bars in ((a)–(d)) are 50 μm. Scale bars for insets in ((b)–(d)) are 20 μm.

Reuse of AIP Publishing content is subject to the terms at: https://publishing.aip.org/authors/rights-and-permissions. Download to IP: 169.235.13.190 On: Fri, 29 Jul 2016 21:22:09

samples at an h-BN growth time of 5, 20, and 30 min for Samples B, C, and D, respectively. As seen from Fig. 1(b) (Sample B), sporadic triangular h-BN flakes have a maximum size of 20 μm and no preferred orientation. This indicates that a short 5-min growth has already resulted in an evident formation of randomly distributed h-BN seeds on the graphene surface. From theoretical calculations,[32] these triangular-shape h-BN domains should end up with a nitrogen-terminated edge due to lower edge energy. At a longer growth duration of 20 min (Sample C), the h-BN flakes are increased both in size and density (Fig. 1(c)). A further increase in h-BN growth time to 30 min led to the connection of these h-BN flakes to form a full-coverage continuous film (Sample D), as shown in Fig. 1(d) and in Fig. S3 (supplementary material). In addition, much larger h-BN domains with a size of $\sim$40 μm can be observed at the edge area of the sample (inset of Fig. 1(d)), which are almost twice the size of the flakes of Sample B (Fig. 1(b)).

Figure 2(a) shows Raman spectra of the as-grown graphene (Sample A) and h-BN/G heterostructure (Sample D). Both spectra exhibit typical G and 2D peaks of graphene, and the G/2D peak ratio indicates the existence of multilayer graphene. An additional peak is also observed at 1368 cm^{-1} for the h-BN/G sample, corresponding to h-BN E_{2g} optical phonon mode.[7] No graphene D peak can be seen, suggesting that the graphene film has negligible defects.[33] Fig. 2(b) shows the UV-Vis absorption spectrum, which was measured based on a transferred h-BN/G film on a sapphire substrate. A strong peak at 203 nm and a weak peak at 270 nm are observed in the absorption spectrum, which are assigned to the optical band gap of h-BN and π-plasmon absorption of graphene, respectively.[15,16] The optical band gap (E_g) value was extracted using the Tauc equation for a direct band gap semiconductor, i.e., $\alpha = C \times (E\text{–}E_g)^{1/2}/E$,[5,34] where α is the absorption coefficient, E is the incident photon energy, and C is the proportionality constant. As shown in Fig. 2(c), the E_g of the h-BN film is around 5.85 eV, which matches well with the reported values of few-layer h-BN.[2,4,7] The wide band gap also implies the excellent insulating characteristics of the as-grown h-BN film. Figs. 2(d), 2(e), and 2(f) show XPS spectra of C1s, N1s, and B1s, respectively. C1s peak at 284.6 eV originates from sp^2 C-C bond,[1] representing the existence of graphene. B1s and N1s exhibit energy positions at 190.6 eV and 397.8 eV, respectively, which are consistent with the reported XPS characteristic lines for h-BN.[1–4] The stoichiometry calculation based on the XPS data gives a B/N ratio of 1.08, suggesting an almost equal composition of B and N elements.

Figure 3(a) shows a cross-sectional TEM image of the h-BN/G heterostructure (Sample D), indicating clear lattice fringes across a total thickness of 32 nm. The average interlayer distance was calculated to be 0.348 nm (for total 92 layers), which is in close agreement with the out-of-plane lattice constants of h-BN and/or graphene.[3] AFM characterization was also carried out on a transferred h-BN/G film on the SiO_2-coated Si substrate (Fig. S4, supplementary material). The line scan of the AFM image indicates that the thickness of the h-BN/G film is around 34 nm, which is comparable with the TEM result. To further differentiate the h-BN and G layers, the depth-profile XPS characterization was performed on the as-grown film (Sample D). 2-keV Ar ion beam was

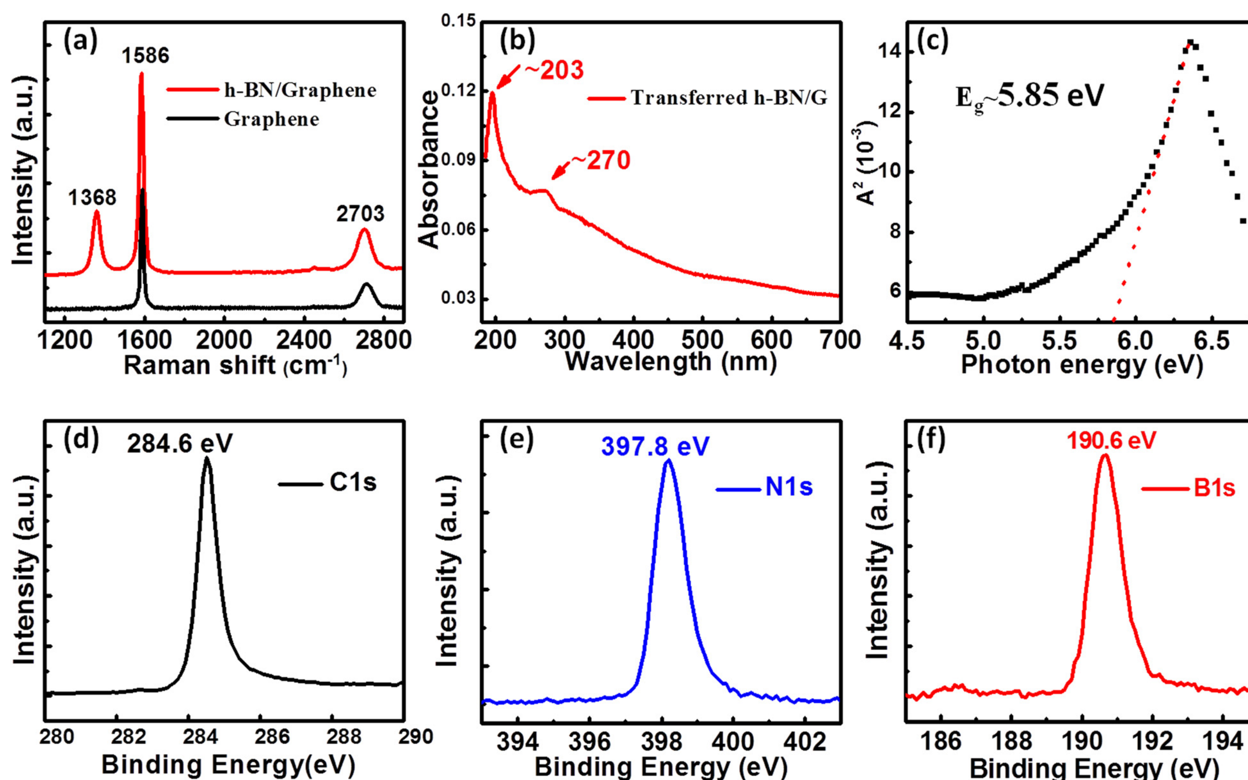

FIG. 2. (a) Raman spectra of the as-grown graphene (Sample A) and h-BN/G heterostructure (Sample D). The G/2D peak ratio in both samples indicates the existence of multilayer graphene. Additional peak is observed besides G and 2D peaks for the h-BN/G sample at 1368 cm^{-1}, corresponding to the E_{2g} optical phonon mode of h-BN. (b) UV-Vis absorption spectrum of a transferred h-BN/G sample on sapphire. (c) α^2 as a function of photon energy. XPS spectra of (d) C1s, (e) N1s, and (f) B1s signals.

Reuse of AIP Publishing content is subject to the terms at: https://publishing.aip.org/authors/rights-and-permissions. Download to IP: 169.235.13.190 On: Fri, 29 Jul 2016 21:22:09

used to sputter a $3 \times 3\,\mathrm{mm}^2$ area with an etching rate of 1 nm per minute. Figs. 3(b) and 3(c) show the evolution of N1s, B1s, and C1s XPS peaks during sputtering. As can be clearly seen, the intensities of the N1s and B1s peaks decrease as the sputtering depth increases, indicating that the top h-BN layer was gradually removed by Ar ion beam sputtering. According to Fig. 3(b), as the sputtering depth reaches ∼5–6 nm, N1s and B1s peaks become negligible, which suggests that the top h-BN film has been entirely removed. On the other hand, the C1s peak intensity increases as the sputtering depth increases and saturates beyond the depth of ∼5–6 nm. This is consistent with the observed evolution of N1s and B1s peaks. Fig. 3(d) shows the calculated relative atomic concentration for B, N, and C as a function of the sputtering depth. As the sputtering depth increases, both N and B concentrations decrease gradually and reach an insignificant percentage at a sputtering depth of ∼5–6 nm, while the C concentration gradually levels up and then becomes steady as the etching depths extends from 6 to 20 nm, where the sputtering experiment was stopped. The steady behavior of C1s peak intensity and C concentration can be understood since the thickness of graphene (∼27–28 nm) is in fact larger than the total sputtering depth (20 nm). Based on all the above information, it can be concluded that the h-BN/G structure has a top h-BN layer with a thickness of ∼5–6 nm and a bottom graphene layer of ∼27–28 nm.

Fig. 4 shows curves of current density (J) versus electric field (E) of 20 Co(foil)/G/h-BN/Co(contact) capacitor devices, which are evenly distributed on the sample. These curves exhibit similar behavior, which suggests that the film has a uniform quality across the sample. As the biases across the capacitors increase, the currents evolve clearly in four regions from the fast-increasing region at the beginning, to the linearly increasing region under moderate biases, to the non-linearly increasing region at higher biases, and finally the to sharp-increasing region. These are corresponding to trap-assisted tunneling,[24,35,36] Ohmic behavior, Fowler-Nordheim tunneling,[37] and dielectric breakdown, respectively. The breakdown electric field (E_{BD}) is shown to be ∼2.5–3.2 MV/cm in an histogram plot in the inset of Fig. 4, which is comparable with the observed values from other epitaxial h-BN films.[6,24,37] Nevertheless, these fields are slightly lower than that obtained from devices based on exfoliated h-BN films.[38] There are two factors: one is associated with the grain boundaries, wrinkles and pinholes possibly existing in the h-BN films, which can provide leakage paths;[24] the other is related to the rough cobalt foil substrate, whose corrugated surface can induce highly localized electric field by the field enhancement factor.[6]

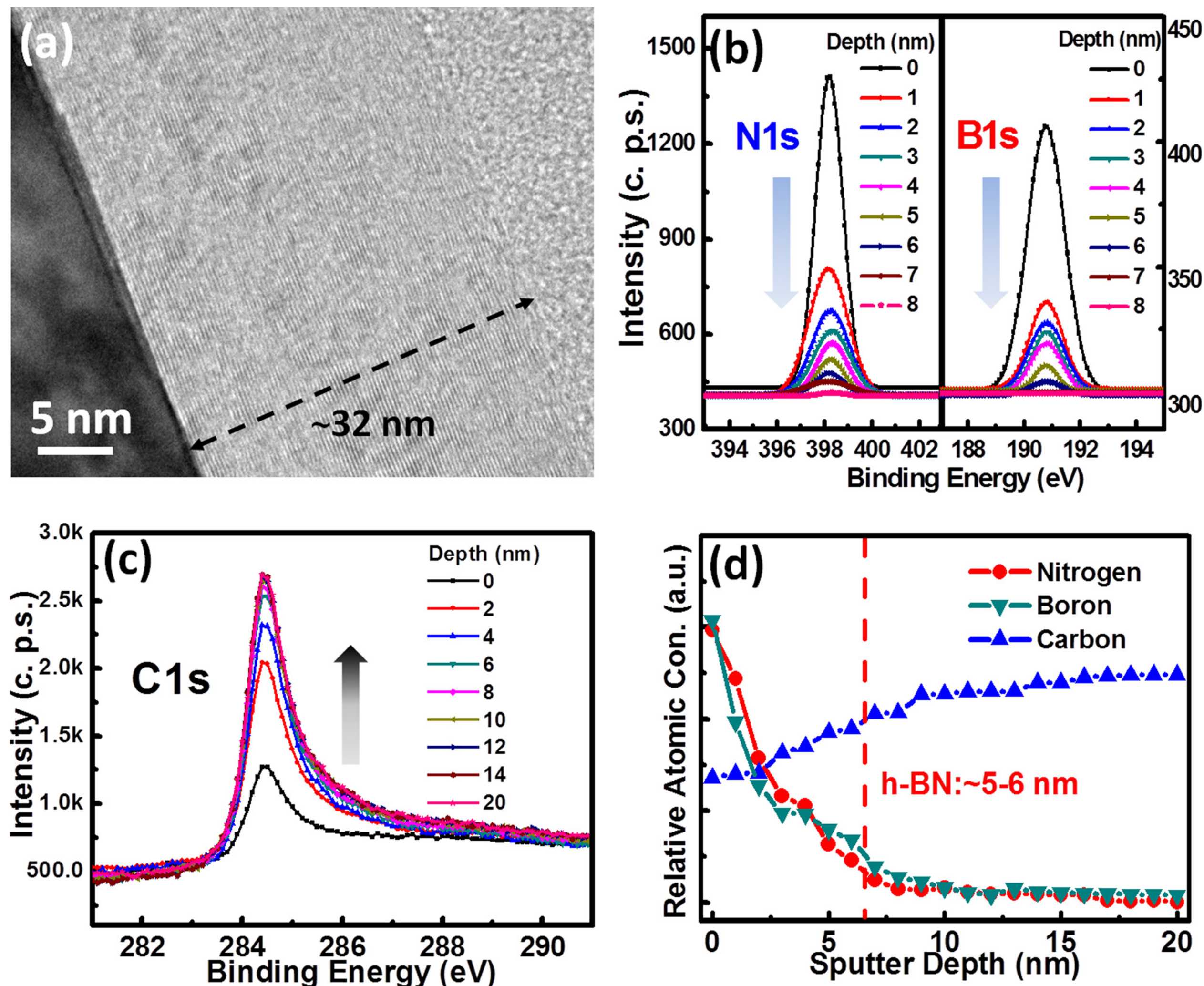

FIG. 3. (a) Cross-sectional TEM image of the as-grown h-BN/G heterostructure on cobalt foil (Sample D). Evolution of (b) N1s, B1s and (c) C1s peaks as a function of sputtering depth in the depth-profile XPS characterization. (d) Relative atomic concentration of B, C and N versus sputtering depth.

Reuse of AIP Publishing content is subject to the terms at: https://publishing.aip.org/authors/rights-and-permissions. Download to IP: 169.235.13.190 On: Fri, 29 Jul 2016 21:22:09

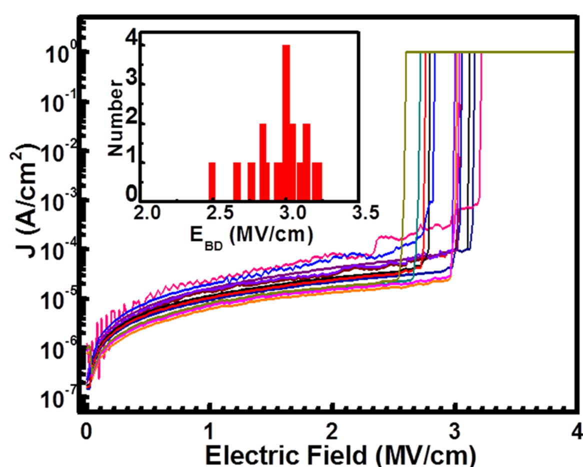

FIG. 4. Current density versus electric field of 20 Co(foil)/G/h-BN/Co(contact) capacitor devices. All devices have the same size of 250 μm × 250 μm. The inset displays histogram plot of E_{BD}.

Specific capacitances of these capacitors were also characterized and analyzed as shown in Fig. S5 in the supplementary material, further demonstrating robust dielectric properties of the h-BN films.

In conclusion, we demonstrated the synthesis of large-area, uniform-quality, and vertically stacked h-BN/G heterostructures on Co foil by sequential deposition of the thin graphite layer and few-layer h-BN through plasma-assisted MBE. Capacitor devices with Co(foil)/G/h-BN/Co(contact) structure were fabricated. Various characterizations including Raman, XPS, AFM, SEM, TEM, UV-Vis absorption, I-V, and C-V were carried out to study the structural, morphological, compositional, resistive, capacitive, and dielectric properties of the heterostructures. The breakdown electric field was estimated to be ∼2.5–3.2 MV/cm, demonstrating that MBE is an alternative tool for growing high-quality h-BN and G/h-BN heterostructure 2D films.

See supplementary material for additional information and figures.

This work was supported by FAME, one of the six centers of STARnet, a Semiconductor Research Corporation program supported by MACRO and DARPA. Cross-sectional TEM specimen preparation using focus ion beam technique and part of TEM imaging were performed at Irvine Materials Research Institute (IMRI) at UC Irvine, using instrumentation funded in part by the National Science Foundation Center for Chemistry at the Space-Time Limit (CHE-082913).

[1]L. Song, L. Ci, H. Lu, P. Sorokin, C. Jin, J. Ni, A. G. Kvashnin, D. G. Kvashnin, J. Lou, B. Yakobson, and P. M. Ajayan, Nano Lett. **10**, 3209 (2010).
[2]Y. Shi, C. Hamsen, X. Jia, K. Kim, A. Reina, M. Hofmann, A. Hsu, K. Zhang, H. Li, Z. Juang, M. Dresselhaus, L. Li, and J. Kong, Nano Lett. **10**, 4134 (2010).
[3]K. K. Kim, A. Hsu, X. Jia, S. M. Kim, Y. Shi, M. Hofmann, D. Nezich, J. F. Rodriguez-Nieva, M. Dresselhaus, T. Palacios, and J. Kong, Nano Lett. **12**, 161 (2012).
[4]G. Kim, A. R. Jang, H. Y. Jeong, Z. Lee, D. J. Kang, and H. S. Shin, Nano Lett. **13**, 1834 (2013).
[5]R. Y. Tay, M. H. Griep, G. Mallick, S. H. Tsang, R. S. Singh, T. Tumlin, E. H. T. Teo, and S. P. Karna, Nano Lett. **14**, 839 (2014).
[6]S. M. Kim, A. Hsu, M. H. Park, S. H. Chae, S. J. Yun, J. S. Lee, D. H. Cho, W. Fang, C. Lee, T. Palacios, M. Dresselhaus, K. K. Kim, Y. H. Lee, and J. Kong, Nat. Commun. **6**, 8662 (2015).
[7]Y. Gao, W. Ren, T. Ma, Z. Liu, Y. Zhang, W.-B. Liu, L.-P. Ma, X. Ma, and H.-M. Cheng, ACS Nano **7**, 5199 (2013).
[8]P. Sutter, J. Lahiri, P. Zahl, B. Wang, and E. Sutter, Nano Lett. **13**, 276 (2013).
[9]C. Dean, A. Young, I. Meric, C. Lee, L. Wang, S. Sorgenfrei, K. Watanabe, T. Taniguchi, P. Kim, K. L. Shepard, and J. Hone, Nat. Nanotechnol. **5**, 722 (2010).
[10]M. P. Levendorf, C. J. Kim, L. Brown, P. Y. Huang, R. W. Havener, D. A. Muller, and J. W. Park, Nature **488**, 627 (2012).
[11]Z. Liu, L. Song, S. Zhao, J. Huang, L. Ma, J. Zhang, J. Lou, and P. M. Ajayan, Nano. Lett. **11**, 2032 (2011).
[12]Z. Liu, L. Ma, G. Shi, W. Zhou, Y. Gong, S. Lei, X. Yang, J. Zhang, J. Yu, K. P. Hackenberg, A. Babakhani, J.-C. Idrobo, R. Vajtai, J. Lou, and P. M. Ajayan, Nat. Nanotechnol. **8**, 119 (2013).
[13]T. Gao, X. Song, H. Du, Y. Nie, Y. Chen, Q. Ji, J. Sun, Y. Yang, Y. Zhang, and Z. Liu, Nat. Commun. **6**, 6835 (2015).
[14]Q. Wu, S. K. Jang, S. Park, S. J. Jung, H. Suh, Y. H. Lee, S. Lee, and Y. J. Song, Nanoscale **7**, 7574 (2015).
[15]J. H. Meng, X. W. Zhang, H. L. Wang, X. B. Ren, C. H. Jin, Z. G. Yin, X. Liu, and H. Liu, Nanoscale **7**, 16046 (2015).
[16]C. Zhang, S. Zhao, C. Jin, A. L. Koh, Y. Zhou, W. Xu, Q. Li, Q. Xiong, H. Peng, and Z. Liu, Nat. Commun. **6**, 6519 (2015).
[17]M. Liu, Y. Li, P. Chen, J. Sun, D. Ma, Q. Li, T. Gao, Y. Gao, Z. Cheng, X. Qiu, Y. Fang, Y. Zhang, and Z. Liu, Nano Lett. **14**, 6342 (2014).
[18]S. M. Kim, A. Hsu, P. T. Araujo, Y. H. Lee, T. Palacios, M. Dresselhaus, J. C. Idrobo, K. K. Kim, and J. Kong, Nano Lett. **13**, 933 (2013).
[19]G. H. Han, J. A. Rodriguez-Manzo, C. W. Lee, N. J. Kybert, M. B. Lerner, Z. J. Qi, E. N. Dattoli, A. M. Rappe, M. Drndic, and A. T. C. Johnson, ACS Nano **7**, 10129 (2013).
[20]L. Liu, J. Park, D. A. Siegel, K. F. McCarty, K. W. Clark, W. Deng, L. Basile, J. Idrobo, A. Li, and G. Gu, Science **343**, 163 (2014).
[21]J. M. Garcia, U. Wurstbauer, A. Levy, L. N. Pfeiffer, A. Pinczuk, A. S. Plaut, L. Wang, C. R. Dean, R. Buizza, A. M. Van Der Zande, J. Hone, K. Watanabe, and T. Taniguchi, Solid State Commun. **152**, 975 (2012).
[22]W. Yang, G. Chen, Z. Shi, C. Liu, L. Zhang, G. Xie, M. Cheng, D. Wang, R. Yang, D. Shi, K. Watanabe, T. Taniguchi, Y. Yao, Y. Zhang, and G. Zhang, Nat. Mater. **12**, 792 (2013).
[23]C. R. Dean, L. Wang, P. Maher, C. Forsythe, F. Ghahari, Y. Gao, J. Katoch, M. Ishigami, P. Moon, M. Koshino, T. Taniguchi, K. Watanabe, K. L. Shepard, J. Hone, and P. Kim, Nature **497**, 598 (2013).
[24]K. K. Kim, A. Hsu, X. T. Jia, S. M. Kim, Y. M. Shi, M. Dresselhaus, T. Palacios, and J. Kong, ACS Nano **6**, 8583 (2012).
[25]L. Britnell, R. V. Gorbachev, R. Jalil, B. D. Belle, F. Schedin, A. Mishchenko, T. Georgiou, L. Eaves, S. V. Morozov, N. M. R. Peres, J. Leist, A. K. Geim, K. S. Novoselov, and L. A. Ponomarenko, Science **335**, 947 (2012).
[26]S. Nakhaie, J. M. Wofford, T. Schumann, U. Jahn, M. Ramsteiner, M. Hanke, and J. M. J. Lopes, Appl. Phys. Lett. **106**, 213108 (2015).
[27]N. Zhan, G. Wang, and J. Liu, Appl. Phys. A **105**, 341 (2011).
[28]Z. Zuo, Z. Xu, R. Zheng, A. Khanaki, J. Zheng, and J. Liu, Sci. Rep. **5**, 14760 (2015).
[29]Z. Xu, R. Zheng, A. Khanaki, Z. Zuo, and J. Liu, Appl. Phys. Lett. **107**, 213103 (2015).
[30]A. A. Tonkikh, E. N. Voloshina, P. Werner, H. Blumtritt, B. Senkovskiy, G. Güntherodt, S. S. P. Parkin, and Yu. S. Dedkov, Sci. Rep. **6**, 23547 (2016).
[31]H. Ago, Y. Ito, N. Mizuta, K. Yoshida, B. Hu, C. M. Orofeo, M. Tsuji, K.-I. Ikeda, and S. Mizuno, ACS Nano **4**, 7407 (2010).
[32]Y. Liu, S. Bhowmick, and B. Yakobson, Nano Lett. **11**, 3113 (2011).
[33]C. Thomsen and S. Reich, Phys. Rev. Lett. **85**, 5214 (2000).
[34]A. Khanaki, H. Abdizadeh, and M. R. Golobostanfard, J. Phys. Chem. C **119**, 23250 (2015).
[35]Y. Hattori, T. Taniguchi, K. Watanabe, and K. Nagashio, ACS Nano **9**, 916 (2015).
[36]Y. Ji, C. Pan, M. Zhang, S. Long, X. Lian, F. Miao, F. Hui, Y. Shi, L. Larcher, E. Wu, and M. Lanza, Appl. Phys. Lett. **108**, 012905 (2016).
[37]G.-H. Lee, Y.-J. Yu, C. Lee, C. Dean, K. L. Shepard, P. Kim, and J. Hone, Appl. Phys. Lett. **99**, 243114 (2011).
[38]A. F. Young, C. R. Dean, I. Meric, S. Sorgenfrei, H. Ren, K. Watanabe, T. Taniguchi, J. Hone, K. L. Shepard, and P. Kim, Phys. Rev. B **85**, 235458 (2012).

Reuse of AIP Publishing content is subject to the terms at: https://publishing.aip.org/authors/rights-and-permissions. Download to IP: 169.235.13.190 On: Fri, 29 Jul 2016 21:22:09